# New Intermetallic Compounds $RE_4Co_2Mg_3$ ($RE$ = Pr, Gd, Tb, Dy) – Syntheses, Structure, and Chemical Bonding

Selcan Tuncel[a], Ute Ch. Rodewald[a], Samir F. Matar[b], Bernard Chevalier[b], and Rainer Pöttgen[a]

[a] Institut für Anorganische und Analytische Chemie, Westfälische Wilhelms-Universität Münster, Corrensstraße 30, 48149 Münster, Germany
[b] Institut de Chimie de la Matière Condensée de Bordeaux (ICMCB), CNRS [UPR 9048], Université Bordeaux 1, 87 avenue du Docteur Albert Schweitzer, 33608 Pessac Cedex, France

Reprint requests to Prof. Dr. R. Pöttgen. E-mail: pottgen@uni-muenster.de

*Z. Naturforsch.* **2007**, *62b,* 162 – 168; received October 20, 2006

The magnesium compounds $RE_4Co_2Mg_3$ ($RE$ = Pr, Gd, Tb, Dy) were prepared by induction melting of the elements in sealed tantalum tubes. The samples were studied by powder X-ray diffraction. The structures of the gadolinium and of the terbium compound were refined from single crystal diffractometer data: $Nd_4Co_2Mg_3$-type, $P2/m$, $Z = 1$, $a = 754.0(4)$, $b = 374.1(1)$, $c = 822.5(3)$ pm, $\beta = 109.65(4)^\circ$, $wR2 = 0.0649$, 730 $F^2$ values for $Gd_4Co_2Mg_3$ and $a = 750.4(2)$, $b = 372.86(6)$, $c = 819.5(2)$ pm, $\beta = 109.48(3)^\circ$, $wR2 = 0.0398$, 888 $F^2$ values for $Tb_4Co_2Mg_3$ with 30 variables each. The $RE_4Co_2Mg_3$ structures are 3 : 1 intergrowth variants of distorted CsCl and $AlB_2$ related slabs of compositions $RE$Mg and $RECo_2$. Characteristic structural features (exemplary for $Tb_4Co_2Mg_3$) are relatively short Tb–Co (271 pm), Co–Co (232 pm) and Mg–Mg (314 pm) distances. The latter are a geometrical constraint of the distortion of the $RE$Mg and $RECo_2$ slabs. Chemical bonding analysis (ELF and ECOV data) for $Gd_4Co_2Mg_3$ reveals strong Gd–Co bonding followed by Mg–Co, while the Mg–Mg interactions can be considered as weak. The Co–Co contacts are only weakly bonding. The bonding and antibonding states are almost filled.

*Key words:* Magnesium, Intermetallics, Crystal Chemistry, Chemical Bonding

## Introduction

Rare earth ($RE$)-transition metal ($T$)-magnesium compounds have technical importance in modern light weight alloys. Addition of misch metal or pure rare earth metals to multinary magnesium based alloy systems induces precipitation hardening [1 – 3, and ref. therein]. Detailed phase analytical investigations of the $RE$-$T$-Mg systems are thus desirable in order to understand the structural, mechanical and physical properties of the ternary phases that can precipitate.

A variety of $RE_xT_yMg_z$ compounds with widely varying crystal chemistry and physical properties have been reported in recent years. A literature overview has been given recently [4]. So far, examples for compositions $RET_4Mg$, $RET_9Mg_2$, $RETMg$, $RETMg_2$, and $RE_2T_2Mg$, and the recently discovered $Nd_4Co_2Mg_3$-type structure [5], are known. While the compounds $RET_4Mg$, $RET_9Mg_2$, and $LaNiMg_2$ have mainly been studied with respect to their hydrogenation properties [6 – 8], the phases $RETMg$ [9, and ref. therein] and $RE_2T_2Mg$ [10] were investigated for their varying magnetic properties. Basic structural units of the latter two series and the $Nd_4Co_2Mg_3$-type structure are transition metal centered trigonal prisms formed by the rare earth and/or magnesium atoms. These prisms can be condensed in different motifs leading to the respective structure types.

During our systematic phase analytical studies of the $RE$-$T$-Mg systems we have obtained new intermetallics $RE_4Co_2Mg_3$ ($RE$ = Pr, Gd, Tb, Dy) with monoclinic $Nd_4Co_2Mg_3$-type structures. The crystal chemistry and chemical bonding of these compounds are reported herein.

## Experimental Section

### *Synthesis*

Starting materials for the preparation of the $RE_4Co_2Mg_3$ samples were ingots of the rare earth metals (Johnson Matthey, > 99.9 %), cobalt powder (Sigma-Aldrich, 100 mesh, > 99.9 %), and a magnesium rod (Johnson Matthey, ∅ 16 mm, > 99.95 %). The surface of the magnesium rod was cut on a turning lathe in order to remove sur-

0932–0776 / 07 / 0200–0162 $ 06.00  · http://znaturforsch.com

| Compound | $a$ (pm) | $b$ (pm) | $c$ (pm) | $\beta$ (deg) | $V$ (nm$^3$) |
|---|---|---|---|---|---|
| $Pr_4Co_2Mg_3$ | 771.8(3) | 383.9(2) | 840.5(4) | 109.90(5) | 0.2342 |
| $Nd_4Co_2Mg_3$ [5] | 765.42(14) | 380.53(5) | 832.47(16) | 109.79(1) | 0.2282 |
| $Sm_4Co_2Mg_3$ [5] | 760.12(15) | 377.11(6) | 826.84(16) | 109.68(1) | 0.2232 |
| $Gd_4Co_2Mg_3$ | 754.0(4) | 374.1(1) | 822.5(3) | 109.65(4) | 0.2185 |
| $Tb_4Co_2Mg_3$ | 750.4(2) | 372.86(6) | 819.5(2) | 109.48(3) | 0.2162 |
| $Dy_4Co_2Mg_3$ | 748.3(4) | 371.07(9) | 816.8(3) | 109.57(3) | 0.2137 |

Table 1. Lattice parameters (Guinier powder data) of the ternary magnesium compounds $RE_4Co_2Mg_3$.

face impurities. The elements were mixed in the ideal 4 : 2 : 3 atomic ratios and arc-welded [11] in small tantalum tubes under an argon pressure of *ca*. 600 mbar. The argon was purified before over molecular sieves, silica gel and titanium sponge (900 K). The tantalum tubes were then placed in a water-cooled quartz sample chamber [12] of a high-frequency furnace (Hüttinger Elektronik, Freiburg, Typ TIG 1.5/300), first heated for 2 min at *ca*. 1300 K and subsequently annealed for another 2 h at *ca*. 920 K, followed by quenching. The temperature was controlled through a Sensor Therm Metis MS09 pyrometer with an accuracy of ±30 K. The brittle reaction products could easily be separated from the crucibles. No reaction with the container material was evident. The $RE_4Co_2Mg_3$ samples are stable in air over months. Polycrystalline material is light gray; single crystals exhibit metallic luster.

The single crystals investigated on the diffractometer and the bulk samples were analyzed by EDX in a LEICA 420 I scanning electron microscope using the lanthanoid trifluorides, cobalt, and magnesium oxide as standards. The EDX analyses revealed no impurity elements and were in agreement with the ideal 4 : 2 : 3 compositions.

*X-Ray powder and single crystal data*

The annealed $RE_4Co_2Mg_3$ samples were studied by X-ray powder diffraction (Guinier technique) using Cu$K_{\alpha 1}$ radiation and $\alpha$-quartz ($a$ = 491.30, $c$ = 540.46 pm) as an internal standard. The Guinier camera was equipped with an imaging plate system (Fujifilm BAS-1800). The monoclinic lattice parameters (Table 1) were obtained from least-squares refinements of the Guinier data. To ensure proper indexing, the experimental patterns were compared to calculated ones [13] using the atomic positions obtained from the structure refinements. For $Gd_4Co_2Mg_3$ and $Tb_4Co_2Mg_3$ the lattice parameters of the powders and the single crystals agreed well.

The samples with gadolinium and terbium were well crystallized. Irregularly shaped single crystals were selected from these samples and first examined by Laue photographs on a Buerger precession camera (equipped with an imaging plate system Fujifilm BAS-1800) in order to establish the crystal quality. Single crystal intensity data were collected at r. t. on a Nonius CAD4 four-circle diffractometer with graphite monochromatized Mo$K_\alpha$ radiation (71.073 pm) and a scintillation counter with pulse height discrimination. The scans were performed in the $\omega/2\theta$ mode. Empirical absorption corrections were applied on the basis of $\Psi$-scan data followed by spherical absorption corrections. All relevant crystallographic data and details for the data collections and evaluations are listed in Table 2.

Table 2. Crystal data and structure refinement for $Gd_4Co_2Mg_3$ and $Tb_4Co_2Mg_3$, $Nd_4Co_2Mg_3$-type, space group $P2/m$, $Z$ = 1.

| Empirical formula | $Gd_4Co_2Mg_3$ | $Tb_4Co_2Mg_3$ |
|---|---|---|
| Molar mass [g mol$^{-1}$] | 819.79 | 826.47 |
| Unit cell dimensions | see Table 1 | see Table 1 |
| Calculated density [g cm$^{-3}$] | 6.23 | 6.35 |
| Crystal size [$\mu$m$^3$] | $20 \times 60 \times 80$ | $20 \times 40 \times 50$ |
| Transm. ratio [max/min] | 0.748 / 0.177 | 0.997 / 0.400 |
| Absorption coefficient [mm$^{-1}$] | 33.7 | 36.1 |
| $F$(000) [e] | 346 | 350 |
| $\theta$ range [deg] | 2 – 30 | 2 – 33 |
| Range in $hkl$ | ±10, ±5, ±11 | ±11, ±5, ±12 |
| Total no. reflections | 2548 | 3128 |
| Independent reflections | 730 | 888 |
| $R_{int}$ | 0.0432 | 0.0233 |
| Reflections with $I \geq 2\sigma(I)$ | 668 | 826 |
| $R_\sigma$ | 0.0292 | 0.0154 |
| Data/parameters | 730 / 30 | 888 / 30 |
| Goodness-of-fit on $F^2$ | 1.182 | 1.230 |
| $R1$ [$I \geq 2\sigma(I)$] | 0.0267 | 0.0165 |
| $wR2$ [$I \geq 2\sigma(I)$] | 0.0638 | 0.0391 |
| $R1$ (all data) | 0.0292 | 0.0188 |
| $wR2$ (all data) | 0.0649 | 0.0398 |
| Extinction coefficient | 0.007(1) | 0.0082(5) |
| Largest diff. peak and hole [e Å$^{-3}$] | 3.57 / −3.20 | 1.19 / −1.46 |

Both data sets revealed no systematic extinctions. In agreement with the symmetry of $Nd_4Co_2Mg_3$, space group $P2/m$ was found to be correct during the structure refinements. The atomic parameters of the neodymium compound [5] were taken as starting values and the structures were refined using SHELXL-97 (full-matrix least-squares on $F_o^2$) [14] with anisotropic atomic displacement parameters for all sites. As a check for possible defects, the occupancy parameters were refined in a separate series of least-squares cycles. All sites were fully occupied within two standard uncertainties. Final difference Fourier syntheses revealed no significant residual peaks (see Table 2). The positional parameters and interatomic distances are listed in Tables 3 and 4. Further details on the structure determinations are available*.

*Details may be obtained from: Fachinformationszentrum Karlsruhe, D-76344 Eggenstein-Leopoldshafen (Germany), by quoting the Registry No's. CSD-417035 ($Gd_4Co_2Mg_3$) and CSD-417036 ($Tb_4Co_2Mg_3$).

Table 3. Atomic coordinates and anisotropic displacement parameters ($pm^2$) for $Gd_4Co_2Mg_3$ and $Tb_4Co_2Mg_3$, space group $P2/m$. $U_{eq}$ is defined as one third of the trace of the orthogonalized $U_{ij}$ tensor. The anisotropic displacement factor exponent takes the form: $-2\pi^2[(ha^*)^2U_{11} + \ldots + 2hka^*b^*U_{12}]$. $U_{12} = U_{23} = 0$.

| Atom | Wyckoff position | $x$ | $y$ | $z$ | $U_{11}$ | $U_{22}$ | $U_{33}$ | $U_{13}$ | $U_{eq}$ |
|---|---|---|---|---|---|---|---|---|---|
| $Gd_4Co_2Mg_3$: | | | | | | | | | |
| Gd1 | 2*n* | 0.60486(4) | 1/2 | 0.81770(4) | 88(2) | 106(2) | 137(3) | 38(1) | 111(1) |
| Gd2 | 2*n* | 0.09363(4) | 1/2 | 0.72520(4) | 100(2) | 136(2) | 133(2) | 32(1) | 125(2) |
| Co | 2*m* | 0.64815(13) | 0 | 0.10485(14) | 100(4) | 150(5) | 173(5) | 12(4) | 150(2) |
| Mg1 | 2*m* | 0.2923(4) | 0 | 0.5017(4) | 118(10) | 197(13) | 167(13) | 57(10) | 158(5) |
| Mg2 | 1*a* | 0 | 0 | 0 | 121(15) | 180(17) | 213(19) | 84(14) | 164(7) |
| $Tb_4Co_2Mg_3$: | | | | | | | | | |
| Tb1 | 2*n* | 0.60462(3) | 1/2 | 0.81870(3) | 96(1) | 90(1) | 115(1) | 39(1) | 99(1) |
| Tb2 | 2*n* | 0.09387(3) | 1/2 | 0.72484(3) | 108(1) | 121(1) | 115(1) | 30(1) | 117(1) |
| Co | 2*m* | 0.64870(10) | 0 | 0.10562(9) | 109(3) | 137(3) | 156(3) | 20(2) | 140(1) |
| Mg1 | 2*m* | 0.2912(3) | 0 | 0.5014(2) | 118(7) | 174(9) | 148(7) | 52(6) | 145(3) |
| Mg2 | 1*a* | 0 | 0 | 0 | 174(12) | 148(12) | 174(11) | 102(10) | 154(5) |

Table 4. Interatomic distances (pm), calculated with the powder lattice parameters in $Gd_4Co_2Mg_3$ and $Tb_4Co_2Mg_3$. Standard deviations are given in parentheses. All distances within the first coordination spheres are listed.

| $Gd_4Co_2Mg_3$ | | | | $Tb_4Co_2Mg_3$ | | | |
|---|---|---|---|---|---|---|---|
| Gd1: | 2 | Co | 289.2(1) | Tb1: | 2 | Co | 287.4(1) |
| | 2 | Co | 294.4(1) | | 2 | Co | 293.2(1) |
| | 2 | Mg2 | 340.9(2) | | 2 | Mg2 | 339.8(1) |
| | 2 | Mg1 | 341.9(3) | | 2 | Mg1 | 341.9(2) |
| | 2 | Mg1 | 351.8(3) | | 2 | Mg1 | 351.3(2) |
| | 1 | Gd2 | 367.0(2) | | 1 | Tb2 | 364.9(1) |
| | 1 | Gd2 | 368.2(2) | | 1 | Tb2 | 367.0(1) |
| | 2 | Gd1 | 374.1(1) | | 2 | Tb1 | 372.9(1) |
| | 1 | Gd1 | 383.2(2) | | 1 | Tb1 | 379.6(1) |
| | 1 | Gd2 | 400.6(2) | | 1 | Tb2 | 399.4(1) |
| Gd2: | 2 | Co | 272.3(1) | Tb2: | 2 | Co | 271.1(1) |
| | 2 | Mg2 | 319.0(1) | | 2 | Mg2 | 318.1(1) |
| | 2 | Mg1 | 331.2(2) | | 2 | Mg1 | 329.1(2) |
| | 2 | Mg1 | 343.5(3) | | 2 | Mg1 | 341.9(2) |
| | 1 | Gd2 | 349.3(2) | | 1 | Tb2 | 347.9(1) |
| | 1 | Gd1 | 367.0(2) | | 1 | Tb1 | 364.9(1) |
| | 1 | Gd1 | 368.2(2) | | 1 | Tb1 | 367.0(1) |
| | 2 | Gd2 | 374.1(1) | | 2 | Tb2 | 372.9(1) |
| | 1 | Gd1 | 400.6(2) | | 1 | Tb1 | 399.4(1) |
| Co: | 1 | Co | 231.8(2) | Co: | 1 | Co | 232.4(2) |
| | 2 | Gd2 | 272.3(1) | | 2 | Tb2 | 271.1(1) |
| | 2 | Gd1 | 289.2(1) | | 2 | Tb1 | 287.4(1) |
| | 2 | Gd1 | 294.4(1) | | 2 | Tb1 | 293.2(1) |
| | 1 | Mg2 | 305.3(2) | | 1 | Mg2 | 303.7(1) |
| | 1 | Mg1 | 311.4(3) | | 1 | Mg1 | 309.9(2) |
| Mg1: | 1 | Co | 311.4(3) | Mg1: | 1 | Co | 309.9(2) |
| | 1 | Mg1 | 314.2(5) | | 1 | Mg1 | 314.2(4) |
| | 2 | Gd2 | 331.2(2) | | 2 | Tb2 | 329.1(2) |
| | 2 | Gd1 | 341.9(3) | | 2 | Tb1 | 341.9(2) |
| | 2 | Gd2 | 343.5(3) | | 2 | Tb2 | 341.9(2) |
| | 2 | Gd1 | 351.8(3) | | 2 | Tb1 | 351.3(2) |
| Mg2: | 2 | Co | 305.3(2) | Mg2: | 2 | Co | 303.7(1) |
| | 4 | Gd2 | 319.1(1) | | 4 | Tb2 | 318.1(1) |
| | 4 | Gd1 | 340.9(2) | | 4 | Tb1 | 339.8(1) |

*Electronic structure calculations: computational framework*

One problem encountered in the theoretical approach of open $4f$ shell rare earth elements within density functional theory DFT [15] is how to account for such states in calculations. This is due to the role played by $4f$ orbitals, *i. e.* contrary to $3d$, localized $4f$ orbitals are not affected by the crystal field and hence by the chemical environment and bonding with neighboring atoms. While $4f$ orbitals can be included within the valence states for La and Ce as well as for the actinides Th($5f$) and U($5f$), this is not the case for Gd and the rare earth elements used in the intermetallic compounds here. A standard procedure for the treatment of localized electrons is to build *pseudo* potentials in which $f$ electrons are kept frozen in the core; the number of $f$ electrons in the core equals the total number of valence electrons minus the formal valence. For instance, Gd has a total of 10 valence electrons (2 *s* electrons, 1 *d* electron and 7 $f$ electrons). However, in all compounds Gd adopts a valency of 3, hence 7 $f$ electrons are placed in the core, when the *pseudo* potential is generated. *Pseudo* potentials [16] truncate the rapid oscillations of the wave function near the core and replace it by soft ones while reproducing the behavior near the valence. This has been assumed in our computations of $Gd_4Co_2Mg_3$ here within the VASP method [17]. Optimization of the structural parameters including lattice parameters and atomic positions was performed until the forces on the atoms were less than 0.02 eV/Å and all the stress components less than 0.003 eV/Å$^3$. An energy cut-off of 268 eV was used for the plane wave basis set. From the results one can get an insight into the electronic distribution within the structure obtained here from the electron localization function (ELF) [18, 19].

With 3 valence electrons expected to be playing the major role in the valence band, we have considered the "isoelectronic" metal Y instead of Gd to further stress the description of the partial density of states DOS and of the chemical bonding using the all electrons scalar relativistic augmented spherical wave (ASW) method [20]. Self-consistency was achieved by an efficient algorithm for convergence acceleration [21], the convergence criteria being $\Delta Q < 10^{-8}$ for the charge transfer and $\Delta E < 10^{-8}$ eV for the total variational energy. The chemical bonding properties were assessed making use of the ECOV criterion [22] implemented with the

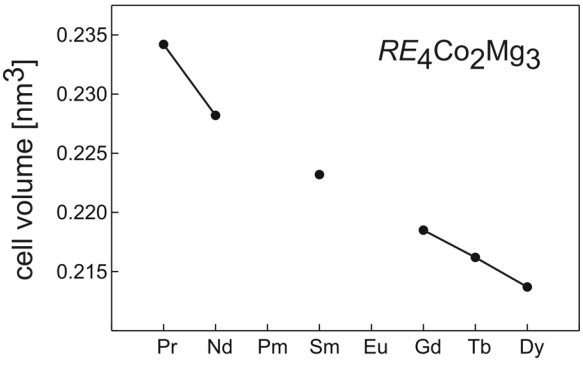


Fig. 1. Course of the unit cell volumes in the series $RE_4Co_2Mg_3$.

ASW method: Negative and positive contributions indicate bonding and antibonding states, respectively, as it will be shown in the plots.

## Discussion

*Crystal chemistry*

The magnesium compounds $RE_4Co_2Mg_3$ (*RE* = Pr, Gd, Tb, Dy) crystallize with the monoclinic $Nd_4Co_2Mg_3$-type structure [5], space group *P*2/*m*, with only seven atoms in the unit cell. As expected from the lanthanoid contraction, the lattice parameters decrease from the praseodymium to the dysprosium compound. The course of the cell volumes is presented in Fig. 1. Also the monoclinic angle shows a slight, but continuous decrease in the same direction. Based on our phase analytical investigations, the series of $RE_4Co_2Mg_3$ compounds seems to be limited to the representatives listed in Table 1. X-Ray powder patterns of samples with the 4 : 2 : 3 starting composition and cerium, respectively holmium, as rare earth metal component revealed the existence of ternary phases with different structure. Detailed investigations on these materials are currently in progress.

A projection of the $Gd_4Co_2Mg_3$ structure is presented in Fig. 2. $Gd_4Co_2Mg_3$ can be considered as a 3 : 1 intergrowth of distorted CsCl and $AlB_2$ related slabs of compositions GdMg and $GdCo_2$, respectively. Thus, the $RE_4Co_2Mg_3$ phases are structurally related to the large family of $RE_2T_2Mg$ intermetallics which are a 1 : 1 intergrowth of similar slabs. This structural relationship has been described in detail in ref. [5].

As a consequence of the lanthanoid contraction, the interatomic distances in $Tb_4Co_2Mg_3$ are slightly smaller than in the prototype $Nd_4Co_2Mg_3$ [5]. This

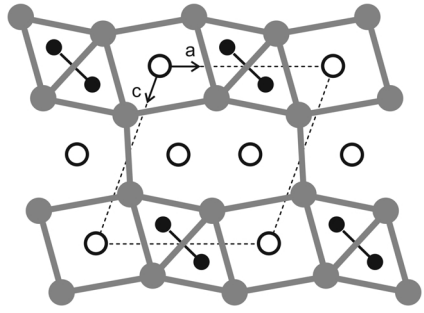


Fig. 2. Projection of the $Gd_4Co_2Mg_3$ structure onto the *xz* plane. All atoms lie on mirror planes at *y* = 0 (Co and Mg) and *y* = 1/2 (Gd), respectively. The gadolinium, cobalt, and magnesium atoms are drawn as medium gray, black filled, and open circles, respectively. The distorted CsCl and $AlB_2$ related slabs are emphasized.

leads to very short Co–Co distances of 232 pm within the $AlB_2$ slab. The latter are significantly shorter than the average Co–Co distance of 250 pm in *hcp* cobalt [23]. In $Zr_2Co_2In$ [24], the Co–Co distance within the $AlB_2$ related slab is much larger (256 pm). This may be a consequence of the higher valence electron concentration in $Zr_2Co_2In$.

Also the Tb2–Co distances of only 271 pm are smaller than the sum of the covalent radii (275 pm) [25] and we can assume significant Tb–Co bonding within the $AlB_2$ related slabs. Between the adjacent CsCl like slabs the Mg–Mg distance is only 314 pm, shorter than the average Mg–Mg distance of 320 pm in *hcp* magnesium [23]. Based on the comparison of the interatomic distances, the main bonding interactions are observed for *RE*–Co, Co–Co, and Mg–Mg.

*Chemical bonding*

The initial crystal structure (Tables 1 and 3) was geometry optimized with a dense enough mesh of k points in the monoclinic first Brillouin zone to allow for convergence and minimum stresses. From the fully relaxed system the monoclinic geometry is preserved with the same space group and a cell volume of 230 Å$^3$, *i. e.* very close to the value in Table 1. From these results one can be confident in examining the distribution of the valence electrons around and between the atomic species. The electron localization function ELF [18] is a real space analysis which allows comparing the electron distribution within a crystal system *versus* the free electron gas.

Fig. 3 shows an ELF plot of two unit cells (*x*, 0, *z* plane at *y* = 0). Here we can trace out the Co–Co

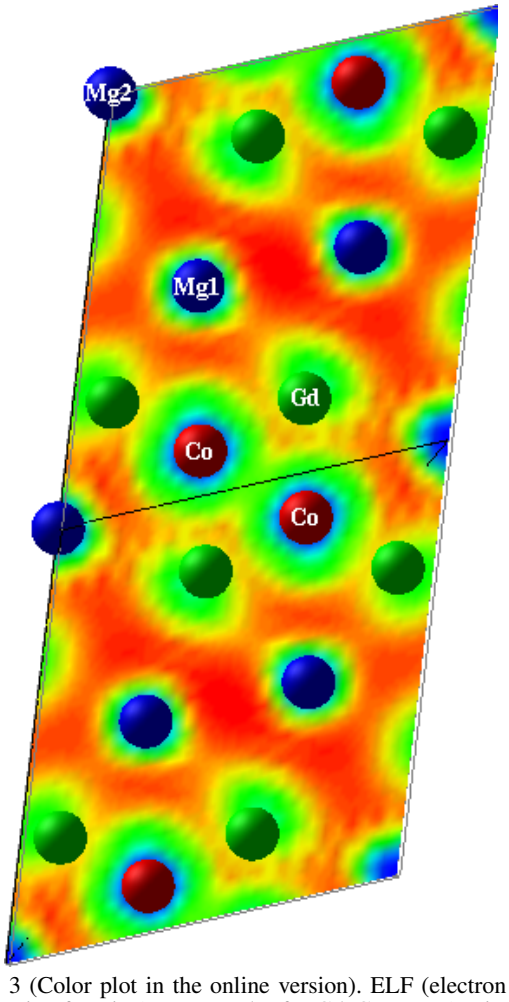


Fig. 3 (Color plot in the online version). ELF (electron localization function) contour plot for $Gd_4Co_2Mg_3$ (projected view of the $x$, 0, $z$ basal plane (2 unit cells) containing the Mg1, Mg2 (blue spheres) and Co atoms; the Gd atoms (green spheres) are above the plane). The electron localization between Co atoms is free electron-like. Blue, green and red contours are for zero localization, free electron-like and full localization, respectively.

pair between the two cells in the middle of the projection. The electron localization between two cobalt atoms is close to free electron behavior (green) but points to some bonding within the $Co_2$ pair. This is further discussed in the chemical bonding section below. Generally, the ELF projection exemplifies the picture that one would expect from a metallic compound, *i. e.* the electrons are localized in between the atoms as it can be followed from the dominant presence of the red contours (high localization). In the immediate neighborhood of the magnesium atoms the blue contours clearly indicate that the magnesium atoms have lost their valence electrons.

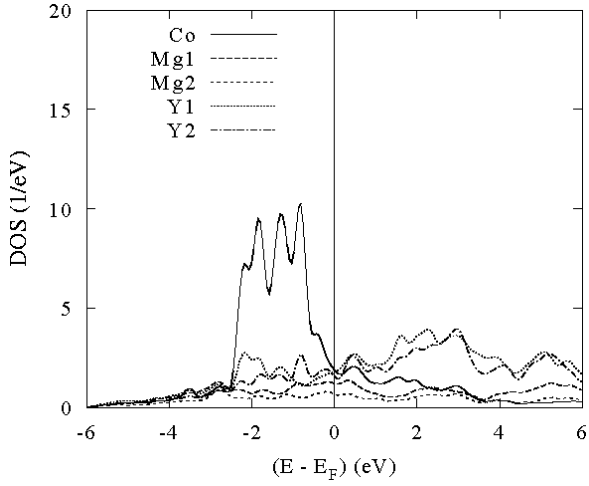


Fig. 4. Site projected DOS of hypothetical "$Y_4Co_2Mg_3$", revealing the major role played by the itinerant electrons (see also the red contours (online version) in the ELF plot of Fig. 3 indicative for strong localization between the atoms).

From the major role played by the valence electrons one can exclude the $4f$ orbitals in the analysis. This can be simulated by replacing gadolinium by yttrium to carry out calculations for a hypothetic compound "$Y_4Co_2Mg_3$" with the cell parameters and atomic positions of $Gd_4Co_2Mg_3$. This was done using the all electrons ASW method described above in order to get an insight into the valence band behavior and the chemical bonding characteristics.

The site projected density of states (DOS) is given in Fig. 4 in which we account for the site multiplicity of each constituent as shown in Table 3. The energy reference along the $x$ axis is with respect to the Fermi energy ($E_F$); this equally applies to the other plots in Figs. 5a and b. The valence band (VB) is dominated by more than half filled low lying Co($3d$) states at $\sim -2$ eV and the largely dispersed *s,p*-like states from other constituents, especially Mg $s$ states. From the features of DOS running similarly along the VB and above $E_F$, the covalence effects are clear, albeit with a low intensity $n(E_F)$. The mixing between itinerant low intensity partial DOS can be inferred from their similar shapes; they are expected to play a role in the chemical bonding. This is especially true for the Y1 and Y2 partial DOS in the energy range $-2$ to $-1$ eV which have a skyline similar to the Co $d$ states so one expects significant mixing between the rare earth (sim-

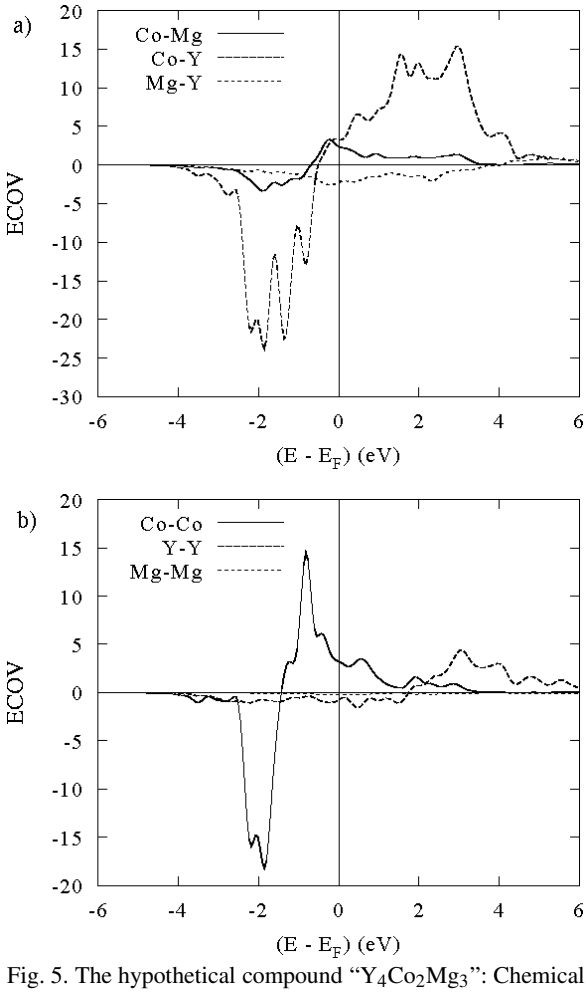


Fig. 5. The hypothetical compound "$Y_4Co_2Mg_3$": Chemical bonding properties derived from the ECOV criterion. a) interactions between different atoms; b) interaction between similar atoms.

ulated by Y here) and Co atoms. This is detailed in Figs. 5a and b showing the interactions between different and similar species, respectively. For sake of clarity and in order to establish comparisons the sites Mg1 and Mg2 are regrouped into "Mg" and Y1 and Y2 into "Y". From Fig. 5a, the largest interaction occurs for Co–Y, followed by Co–Mg. For both interactions, the states are bonding nearly all over the VB; they start to be antibonding just below $E_F$. One can thus propose that this structure type is mainly stabilized through these two interactions. Their antibonding counterparts are found above the Fermi level. The Mg–Y interactions are weak. They are bonding throughout the VB and even at and above $E_F$. This is due to the filling of the orbitals available for the interaction which, in the case of Mg and Y, can receive mainly bonding electrons. An interesting structural feature are the $Co_2$ pairs with a short Co–Co distance of 232 pm. Fig. 5b indeed shows that the Co–Co interaction is the strongest (with a negative ECOV at around $-2$ eV). However, due to the extensive filling of Co(*d*) states, the antibonding counterpart immediately follows so that the Co–Co interaction cannot be the determining fact for the stability of the structure, *i. e.* the bonding part is compensated by the antibonding part, as is also illustrated by the green ELF contours between cobalt spheres (Fig. 3). A similar bonding situation was observed for the $Ni_2$ pair in $Sc_2Ni_2In$ [26] (with a tendency for a closed-shell interaction).

On the contrary, the Mg–Mg and Y–Y interactions are weak. Although they are bonding all over the VB, they need to be considered as negligible. The short Mg–Mg distances are most likely a geometrical constraint of the distortion of the *RE*Mg and *RE*$Co_2$ slabs.

## Conclusions

The intermetallic compounds $RE_4Co_2Mg_3$ (*RE* = Pr, Gd, Tb, Dy) crystallize with a 3 : 1 intergrowth variant of CsCl and $AlB_2$ related slabs. The structures are stabilized through strong *RE*–Co and Mg–Co interactions. In contrast to the related $RE_2T_2Mg$ series, the $RE_4Co_2Mg_3$ compounds have two crystallographically independent *RE* sites which may lead to interesting magnetic properties. Their determination is currently in progress.

*Acknowledgements*

We thank Dipl.-Chem. F. M. Schappacher for the work at the scanning electron microscope. This work was financially supported by the Deutsche Forschungsgemeinschaft. B. C. and R. P. are indebted to EGIDE and DAAD for research grants within the PROCOPE programs (11457RD and D/0502176). Computational facilities provided on the supercomputers of the University Bordeaux 1 (M3PEC) are acknowledged.

[1] K. U. Kainer (ed.), *Magnesium*, Proceedings of the 6th International Conference on Magnesium Alloys and their Applications, Wiley-VCH, Weinheim (Germany) **2004**.

[2] R. Pöttgen, R.-D. Hoffmann, *Metall* **2004**, *58*, 557.

[3] N. Hort, Y. Huang, K. U. Kainer, *Adv. Eng. Mater.* **2006**, *8*, 235.

[4] S. Tuncel, R.-D. Hoffmann, B. Chevalier, S. F. Matar, R. Pöttgen, *Z. Anorg. Allg. Chem.*; in press.
[5] S. Tuncel, R.-D. Hoffmann, B. Heying, B. Chevalier, R. Pöttgen, *Z. Anorg. Allg. Chem.* **2006**, *632*, 2017.
[6] K. Kadir, T. Sakai, I. Uehara, *J. Alloys Compd.* **2000**, *302*, 112.
[7] P. Solokha, V. Pavlyuk, A. Saccone, S. De Negri, W. Prochwicz, B. Marciniak, E. Różycka-Sokołowska, *J. Solid State Chem.* **2006**, *179*, 3073.
[8] G. Renaudin, L. Guénée, K. Yvon, *J. Alloys Compd.* **2003**, *350*, 145.
[9] J. Gegner, T. C. Koethe, H. Wu, H. Hartmann, T. Lorenz, T. Fickenscher, R. Pöttgen, L. H. Tjeng, *Phys. Rev. B* **2006**, *74*, 073102.
[10] M. Lukachuk, R. Pöttgen, *Z. Kristallogr.* **2003**, *218*, 767.
[11] R. Pöttgen, Th. Gulden, A. Simon, *GIT Labor Fachzeitschrift* **1999**, *43*, 133.
[12] D. Kußmann, R.-D. Hoffmann, R. Pöttgen, *Z. Anorg. Allg. Chem.* **1998**, *624*, 1727.
[13] K. Yvon, W. Jeitschko, E. Parthé, *J. Appl. Crystallogr.* **1977**, *10*, 73.
[14] G. M. Sheldrick, SHELXL-97, Program for Crystal Structure Refinement, University of Göttingen (Germany) **1997**.
[15] W. Kohn, L. J. Sham, *Phys. Rev. A* **1965**, *140*, 1133, and P. Hohenberg, W. Kohn, *Phys. Rev. B* **1964**, *136*, 864.
[16] D. Vanderbilt, *Phys. Rev. B* **1990**, *41*, 7892.
[17] G. Kresse, J. Hafner, *Phys. Rev. B* **1993**, *47*, 558; G. Kresse, J. Hafner, *Phys. Rev. B* **1994**, *49*, 14251; G. Kresse, J. Furthmüller, *Comput. Mat. Sci.* **1996**, *6*, 15; G. Kresse, J. Furthmüller, *Phys. Rev. B* **1996**, *54*, 11169.
[18] D. Becke, K. E. Edgecombe, *J. Chem. Phys.* **1990**, *92*, 5397.
[19] R. Weihrich, S. F. Matar, E. Betranhandy, V. Eyert, *Solid State Sci.* **2003**, *5*, 701.
[20] A. R. Williams, J. Kübler, C. D. Gelatt Jr., *Phys. Rev. B* **1979**, *19*, 6094; V. Eyert, *Int. J. Quant. Chem.* **2000**, *77*, 1007.
[21] V. Eyert, K. H. Höck, *Phys. Rev. B* **1998**, *57*, 12727.
[22] G. Bester, M. Fähnle, *J. Phys.: Condens. Matter* **2001**, *13*, 11541.
[23] J. Donohue, *The Structures of the Elements*, Wiley, New York (USA) **1974**.
[24] R. Pöttgen, G. Kotzyba, *Z. Naturforsch.* **1996**, *51b*, 1248.
[25] J. Emsley, *The Elements*, Oxford University Press, Oxford (U.K.) **1999**.
[26] R. Pöttgen, R. Dronskowski, *Z. Anorg. Allg. Chem.* **1996**, *622*, 355.